Experimental Brain Research (2019) 237:3333–3350
https://doi.org/10.1007/s00221-019-05675-z

RESEARCH ARTICLE

Morphological and electrophysiological properties of serotonin neurons with NMDA modulation in the mesencephalic locomotor region of neonatal ePet-EYFP mice

Renkai Ge[1,3] · Ke Chen[1] · Yi Cheng[2] · Yue Dai[1,2]

Received: 2 December 2018 / Accepted: 7 November 2019 / Published online: 12 November 2019

Abstract

The mesencephalic locomotor region (MLR) is an essential area for initiation of locomotion. Its functional roles and circuits underlying locomotion have been studied intensively in many species. Studies suggest that cuneiform nucleus and pedunculopontine nucleus (PPN) are two core regions in the MLR for locomotion. However, it remains unclear about cellular components and morphological and intrinsic membrane properties of the neurons in these regions, especially the serotonergic neurons. Using neonatal ePet-EYFP transgenic mice and immunofluorescent technique, we demonstrated existence of 5-HT neurons in the MLR and discovered that 5-HT neurons distributed mainly in the caudal PPN. 5-HT neurons were heterogeneous in MLR and had three types of firing pattern (single spike, phasic and tonic) and two subtypes of morphology (pyramidal and stellate). We measured parameters of 5-HT neurons ($n = 35$) including resting membrane potential (-69.2 ± 4.2 mV), input resistance (1410.1 ± 616.9 MΩ), membrane capacitance (36.4 ± 14.9 pF), time constant (49.7 ± 19.4 ms), voltage threshold (-32.1 ± 7.4 mV), rheobase (21.3 ± 12.4 pA), action potential amplitude (58.9 ± 12.8 mV) and half-width (4.7 ± 1.1 ms), afterhyperpolarization amplitude (23.6 ± 10.4 mV) and half-decay (331.6 ± 157.7 ms). 5-HT neurons were intrinsically different from adjacent non-5-HT neurons and less excitable than them. Hyperpolarization-activated inward currents and persistent inward currents were recorded in 5-HT neurons. NMDA increased excitability of 5-HT neurons, especially the tonic-firing neurons, accompanied with depolarization of membrane potential, hyperpolarization of voltage threshold, reduction of afterhyperpolarization half-decay, and left-shift of frequency–current relationship. This study provided insight into the distribution and properties of 5-HT neurons in the MLR and interaction between serotonergic and glutamatergic modulations.

Keywords Serotonin neurons · Mesencephalic locomotor region · Membrane property · Excitability · NMDA modulation

Introduction

Locomotion is a fundamental motor behavior initiated by a cluster of neurons in the mesencephalic locomotor region (MLR) and implemented by the central pattern generators (CPGs) in spinal cord (Noga et al. 2003; Harris-Warrick 2010; Cheng et al. 2019). The MLR, a supraspinal center for initiating and modulating locomotion, was first described by Shik and colleagues in 1966 (Shik et al. 1966). And since then the MLR has been studied intensively in many species in which it was shown that electrical or pharmacological stimulation of the MLR could initiate locomotion and change the locomotor speed and pattern. As the center for initiation of locomotion, the key functions of the MLR have been well conserved in the process of biological evolution from lower vertebrates such as lamprey to mammals such as humans (Garcia-Rill et al. 1985; Takakusaki et al. 2003;

Communicated by Steve Edgley.

✉ Yue Dai
ydai@tyxx.ecnu.edu.cn

[1] Shanghai Key Laboratory of Multidimensional Information Processing, School of Communication and Electronic Engineering, East China Normal University (ECNU), Shanghai 200241, China

[2] Key Laboratory of Adolescent Health Assessment and Exercise Intervention of Ministry of Education, School of Physical Education and Health Care, East China Normal University, Shanghai 200241, China

[3] School of Physical Education and Health Care, East China Jiaotong University, Nanchang 330013, China

Grillner and El Manira 2015; Grillner and Robertson 2016; Noga et al. 2017a, b; Caggiano et al. 2018). Results from early studies showed that the locomotion commands originated in the MLR, bilaterally descended to ventral medullary area (Shefchyk et al. 1984; Noga et al. 2003), and then went through the ventral funiculus to activate spinal CPGs neurons (Steeves and Jordan 1980). However, the exact neuron populations and organization of the circuits of the pathways still remain unclear. Using new approaches such as transgenic models, optogenetics and viral tools the mystery of the MLR is being uncovered. It is shown recently that the cuneiform nucleus (CnF) and the pedunculopontine nucleus (PPN), two core components of the MLR, contribute separately to the control of high-speed synchronous-gait locomotion and slower alternating-gait locomotion (Josset et al. 2018b). The CnF modulates the high locomotor speed via the pathway that receives inputs from the periaqueductal grey and inferior colliculus and then sends outputs to lateral paragigantocellular nucleus. In contrast, the PPN receives inputs from the basal ganglia and motor cortex and then produces outputs to lateral paragigantocellular nucleus to form the command pathway that encodes slow locomotor speeds (Caggiano et al. 2018). These studies unveil the functional different pathways of the MLR. But the neurons which are composed of the CnF and PPN need to be further explored. The neurons in CnF and PPN are diverse in neuronal types and composed of cholinergic (Wang and Morales 2009), glutamatergic (Ryczko et al. 2016), GABAergic (Ford et al. 1995), and serotonergic (Beitz 1982; Molliver 1987; Ge et al. 2017) neurons. As an essential neurotransmitter serotonin (5-HT) plays a critical role in initiating locomotion (Schmidt and Jordan 2000). It was shown recently that electrical stimulation of MLR induced the 5-HT release in spinal cord (Noga et al. 2017b). 5-HT neurons in brainstem can be classified into 9 clusters (B1–B9) based on their projections in CNS (Dahlstroem and Fuxe 1964). The serotonergic innervation of the spinal cord is from not only the medullary groups of B1–B3, but also the midbrain groups of B7 and B9 (Bowker et al. 1981). 5-HT neurons of B1–B3 descending to the spinal cord are thought to be the key components for controlling locomotion (Slawinska et al. 2014). Using ePet-EYFP transgenic mice (Scott et al. 2005) where the EYFP was expressed specifically in 5-HT neurons we demonstrated recently that the EYFP positive neurons scattered in the PPN (Ge et al. 2017). However, little is known about the distributional, morphological, electrophysiological, and modulatory properties of these 5-HT neurons due to technical difficulty in identifying these neurons in this region.

In addition to initiation of locomotion, MLR is shown to regulate the locomotor speed and gait through glutamatergic excitatory neurons in the MLR (Caggiano et al. 2018). NMDA alone or together with 5-HT can induce locomotion (Grillner et al. 1981). However, the NMDA-mediated locomotion can be inhibited by 5-HT receptor antagonist (MacLean et al. 1998), implicating that NMDA-induced locomotion may be 5-HT dependent. However, the details of the interaction between serotonergic and glutamatergic systems for initiation or control of locomotion in the MLR remain unknown. Using ePet-EYFP transgenic mice, whole-cell patch-clamp, and immunofluorescence techniques we investigated electrophysiological and morphological properties of 5-HT neurons in the MLR, analyzed the anatomic distribution of 5-HT neurons in this region, and explored the modulation properties of 5-HT neurons by NMDA. Our study indicated that 5-HT neurons were heterogeneously scattered in the PPN. They were electrophysiologically different from the adjacent non-5-HT neurons, and NMDA increased the neuronal excitability of the 5-HT neurons. Preliminary data was published in abstract form (Ge et al. 2017).

Materials and methods

Animals and ethical approval

The animal protocols were reviewed and approved by the East China Normal University Laboratory Animal Center and Animal Experiment Ethics Committee. Pet-1, an ETS domain transcription factor, was a precise marker of developing and adult 5-HT neurons. The ePet-EYFP transgenic neonatal mice of either sex were used in this study. In order to minimize the influence of neuron maturation on morphological and electrophysiological properties, all the neurons recorded in this study were collected from mice of 4–6 days, and mice of 1–11 days were used to qualitatively and quantitatively study the distribution of serotonin neurons in the MLR. Five mice (p 4–6) were used for immunofluorescence. The mice were bred through male ePet-cre transgenic mice crossing with female R26-stop-EYFP mice (Jackson Lab, USA ePet-cre: Stock No:012712; R26-stop-EYFP: Stock No:006148).

Preparation of slices

The procedure for the preparation of mouse brain slices was similar to that previously reported (Dai et al. 2009a; Dai and Jordan 2011). Briefly, the mice were anesthetized by the diethyl ether, quickly decapitated and brains were dissected. Cerebral cortices and cerebellums were removed and the mesencephalons remained. 200 µm transverse slices and 150 µm sagittal slices were cut using Leica (VT 1000E Germany) vibrating microtome. CnF and PPN were the two core constituents of the MLR. According to the brain stereogram of the mice plotted by George Paxinos et al. (2014), the brain 200 µm transverse slices containing

CnF and PPN (3.0–3.4 mm caudal to bregma, Fig. 1a–c) were transferred to the recording aCSF for at least 1 h at room temperature before the patch-clamp recordings. In addition, a series of consecutive 30 µm transverse slices were cut for study of distribution of 5-HT neurons in the MLR. The number of 5-HT neurons was estimated by summing up the 5-HT neurons in the MLR from all the slices for each mouse.

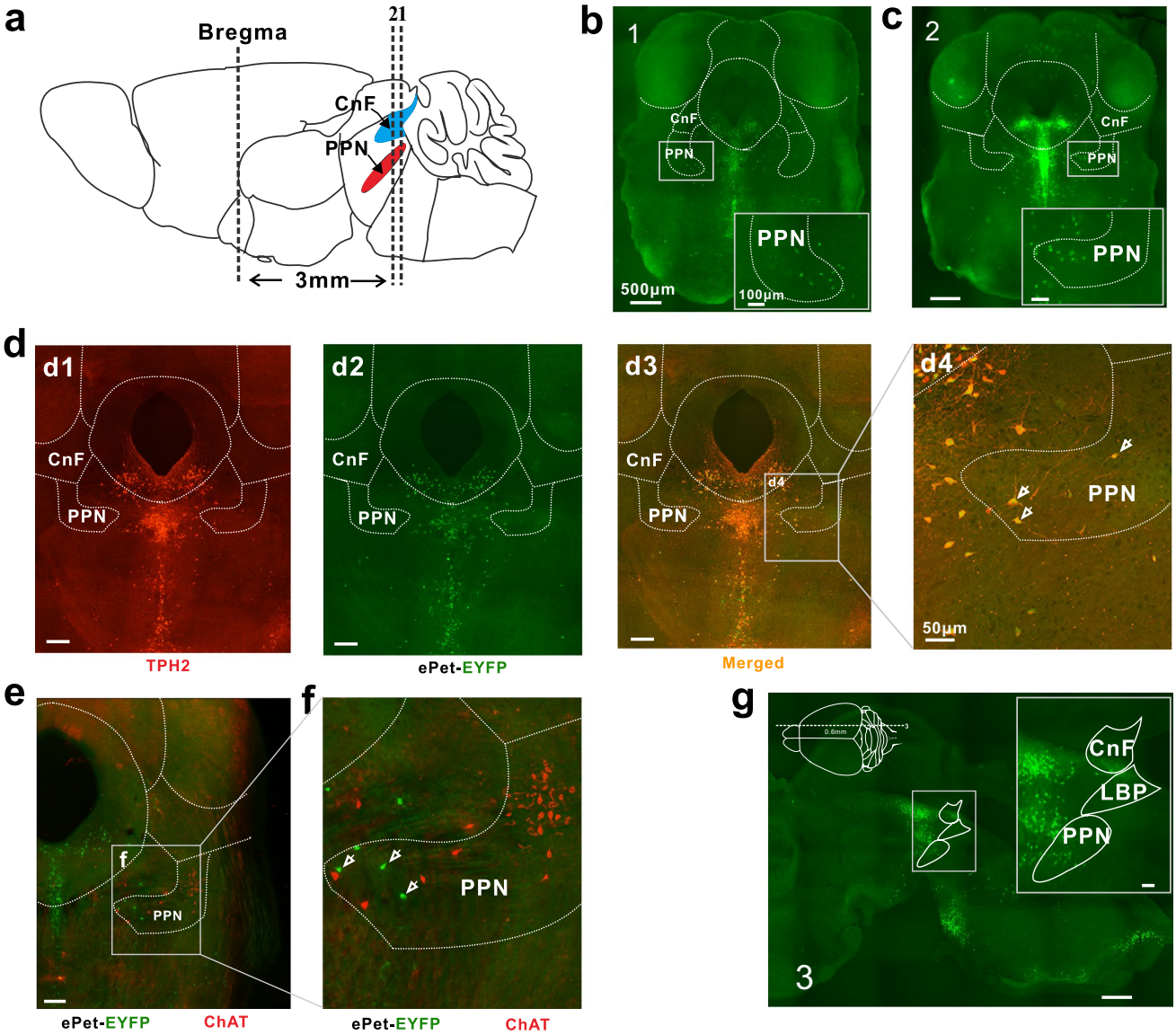

Fig. 1 Distribution of 5-HT neurons in the MLR. **a** Schematic drawing of the mouse brain. The transverse brain slices containing MLR were collected from the area (3.0–3.4 mm caudal to bregma) indicated by dotted lines, which were marked 1 and 2, respectively, from caudal to rostral. **b**, **c** Example fluorescence images were collected from the sites indicated in **a**. The positions of the CnF and PPN were delineated by dotted lines. The green spots in the pictures were EYFP positive 5-HT neurons. 5-HT neurons sparsely distributed in the PPN, rarely in the CnF as shown in low images (**b**, **c**) and high-magnification images (Fig. 1b, c enlarged images in the lower right corner). **d** EYFP positive neurons were 5-HT positive by staining TPH2. d1 Fluorescence image of staining of TPH2 (1:200, ab184505, Abcam). d2 Fluorescence image of EYFP positive neurons. d3 Merged image of d1 and d2. d4 Enlarged image in d3 showed colocalization of EYFP and TPH2 positive neurons in PPN, and arrowheads showed these neurons. **e** Identification of PPN by staining ChAT (red, 1:1000, ab6168, Abcam) and localization of EYFP positive neurons (green) in this region. Arrowheads showed 5-HT neurons in PPN. **f** Enlarged image in Fig. 1e showed existence of EYFP positive neurons in PPN. **g** An example fluorescence image of 150 µm thickness sagittal brain slice of ePet-EYFP transgenic neonatal (P8) mice. Enlarged image in the upper right corner showed the distribution of 5-HT neurons in PPN

Whole-cell patch-clamp recording

The slices were transferred to a recording chamber mounted in the stage of an upright Olympus BX50 microscope fitted with differential interference contrast (DIC) optics and epifluorescence. The chamber was perfused with recording aCSF at a rate of 1–2 mL/min via a gravity drive irrigation system, bubbled with 95% O_2 and 5% CO_2. Anatomical positions of the CnF and PPN were identified at 10 × magnification according to the brain stereogram of the mice in the present study (George Paxinos et al. 2014). For instance, the center of PPN in Fig. 1c is approximately 3.2 mm caudal to bregma, 0.7 mm lateral to the midline and 2.1 mm below the dura mater, and the center of CnF is 1 mm lateral to the midline and 1.3 mm below the dura mater. The EYFP positive 5-HT neurons in the CnF and PPN were identified at 40× magnification using epifluorescence and images were collected (Hamamatsu camera controller C2400 and ARGUS image processor). The visualized neurons were patched. The pipette electrodes were pulled from borosilicate glass (WPI 1B150F-4) using a VT1000S Sutter puller and had resistances of 5–8 MΩ when filled with intracellular solution. A MultiClamp 700B patch-clamp amplifier, Axon Digidata 1550 A/D converter, Minidigi 1B, and pClamp (10.7) software (all from Molecular Devices) were used for data acquisition.

Measurement of membrane parameters

The membrane properties measured and calculated in this study had been described in our previous studies (Dai et al. 2002, 2009a). Briefly, the rheobase was determined by step currents with 0.5 s duration and 5 pA for each step. The minimum step which could evoke a single spike or repetitive firing was taken as rheobase. The voltage threshold (*V*th) was defined as the membrane potential at which the rising rate of $dV/dt \geq 10$ mV/ms. The *V*th reported in this study was calculated from the spike averaged from the first three spikes of firings evoked by rheobase. The resting membrane potential (Em) was monitored throughout the recordings. The reported Em in this paper was calculated from the membrane potentials averaged over 100 ms prior to the step currents used for determining the rheobase. The measurements of action potential (AP) and afterhyperpolarization (AHP) properties were based on the averaged spike evoked by rheobase. The *V*th was used as reference value to measure the AP height and half-width and AHP depth and duration. The input resistance (R_{in}) was calculated by the mean value of membrane potentials divided by the amplitude of the corresponding negative step current (0.5 s duration, − 5 pA step). The membrane time constant (τ_m) was determined by fitting an exponential function with form of $f(t) = A_0 + A1*\mathrm{Exp}(-t/\tau_m)$ to the averaged voltage responses to a train of 5 pulses (0.5 ms, − 500 pA, 250 ms interval). Membrane capacitance (C_m) was calculated by formula $C_m = \tau_m/\mathrm{Rin}$. Step currents with duration of 3 s and step of 10 pA were injected into the cells to determine the *F–I* relations. The Ih-mediated depolarizing sag was recorded through a series of 1.5 s step currents with step of − 10 pA. The sag was defined as the voltage difference between the instantaneous voltage (V_{ins}) and steady state voltage (V_{ss}) and calculated by the formula: $\mathrm{sag} = V_{ss} - V_{ins}$ (Fig. 5e). The sag elicited in the − 30 pA, − 20 pA and − 10 pA steps were calculated in all cell ($n = 7$), respectively. (Dai and Jordan 2010a). The persistent inward currents were recorded by applying a series of slow voltage bi-ramps with a duration of 10 s, a step of 20 or 30 mV, and a holding potential of − 70 mV. The leak current was subtracted from the recordings before the biophysical parameters of PIC were calculated, including PIC amplitude, onset voltage. Difference of PICs between conditions (control, drugs, washout, etc.) were calculated from the PICs evoked by the same slope of voltage ramp in each individual condition. Whole-cell patch recordings were made in voltage-clamp mode with series resistance (10–30 MΩ) compensation by 80-85% and in current clamp mode with bridge balance and capacitance compensation. The liquid junction potential was calculated as 6.7 mV with pH value of recording solution adjusted to 7.3 by KOH, osmolarity adjusted to 305 mOsm by sucrose. This value was corrected in the reported data. Data were low-filtered at 3 kHz and sampled at 10 kHz. During the experiment, the recording protocols were repeated three to five times in each condition (control, drugs, and washout, etc.) with 30–60 s between two successive recordings and 1–5 min between two successive protocols.

The screening criteria for electrophysiological data analysis in present study was that the resting membrane potential was lower than − 55 mV, input resistance bigger than 400 MΩ, and the overshoot of the action potential (above zero) higher than 10 mV. Clampfit 10.7 was used to analyze the data. All recordings were made at room temperature (20–22 °C).

In this study, a MultiClamp 700B patch-clamp amplifier was used to acquire intracellular data. The access resistances of the recordings were corrected by bridge balance in current clamp mode and by 80–95% series resistance compensation in voltage-clamp mode before the intracellular recordings. Therefore, no correlation could be established between the access resistances and the parameters we calculated, suggesting that the membrane properties and firing patterns of the neurons characterized in this study should reflect the intrinsic properties of the neurons rather than variations in recording quality.

Imaging and Sholl analysis

For morphological analysis, the EYFP positive 5-HT neurons were patched and labeled using pipette electrodes filled with intracellular solution containing 3% tetramethylrhodamine. After 5–10 min of staining, images of the labeled neurons were immediately taken by a Nikon Eclipse Ni fluorescence microscopy with a Nikon DS-Ri2 color digital camera at 540–580 nm and 465–495 nm excitation wavelengths, separately.

The Sholl analysis was used to quantify neuronal dendritic complexity. It created a series of concentric circles around the focus of a neuronal dendritic arbor, and counted how many times connected voxels defining the dendritic arbor intersect the sampling circles as well as the length of each dendritic arbor segment within each radii. In addition, the dendritic branches, dendritic terminals, diameter of soma, and primary dendritic segments were analyzed in the same labeled neuron. For Sholl analysis in this study, the center of concentric spheres was defined as the center of the soma, and a 25 µm radius interval was used. The Sholl analysis was obtained using Image J software (1.52 g) loaded with Sholl Analysis (http://imagej.net/Sholl_Analysis) and Neuron J plugins (http://imagej.net/Sholl_Analysis) (Meijering et al. 2004).

Immunofluorescence

The neonatal mouse brainstem tissues were fixed with 4% paraformaldehyde at 4 °C for 6 h. After fixation, tissues were embedded in low-melting agarose, and cut into 30 µm transverse sections with Leica vibrating microtome (VT 1000E, Germany). Sections were permeabilized with 0.3% Triton X-100 (Sinopharm Chemical Reagent Co., Ltd) and blocked with 5% bovine serum albumin (BSA, Sinopharm Chemical Reagent Co., Ltd) in 0.1 M PBS (Sinopharm Chemical Reagent Co., Ltd) for 30 min. The sections were incubated with primary antibodies: rabbit anti-TPH2 (1:200, ab184505, Abcam) or rabbit anti-ChAT (1:1000, ab6168, Abcam) diluted in 5% BSA in PBS at 4 °C overnight. Afterwards, the sections were washed with 0.1 M PBS (3 times, 5 min each time) and incubated with secondary antibodies: goat anti-rabbit IgG (1:100, A-11012, Invitrogen) diluted in 5% BSA in PBA for 1 h at room temperature. After washing with 0.1 M PBS, the stained neurons were photographed with a fluorescence microscope using 10 × and 20 × objectives (Nikon Eclipse Ni fluorescence microscopy).

Solutions and chemicals

Dissecting artificial cerebrospinal fluid (aCSF) contained (in mM): NaCl (25), sucrose (188), KCl (1.9), NaH_2PO_4 (1.2), $MgSO_4$ (10), $NaHCO_3$ (26), kynurenic acid (1.5), glucose (25), and $CaCl_2$ (1.0).

Recording aCSF containing (in mM): NaCl (125), KCl (2.5), $NaHCO_3$ (26), NaH_2PO_4 (1.25), glucose (25), $MgCl_2$ (1), and $CaCl_2$ (2.0), TEA (10, only in voltage-clamp mode).

Intracellular solution containing (in mM): K-gluconate (130), NaCl (10), HEPES (10), $MgCl_2$ (2), Mg-ATP (5), and GTP (0.5), TEA-Cl (20, only in voltage-clamp mode).

The pH of these solutions was adjusted to 7.3 with HCl. Osmolarity was adjusted to 305 mOsm by adding sucrose to the solution.

Drugs

NMDA (10–15 µM, Sigma) was agonist of NMDA receptor. Fluorescent dye Dextran, tetramethylrhodamine (3%, Thermofisher) was used to intracellularly label the 5-HT neurons.

Statistical analysis

Microsoft Excel (Office 2016) was used for data formatting and statistical analysis was carried out using IBM SPSS statistics (version 22). The data were presented in mean ± SD. Unpaired two tailed Student's *t* test was conducted for analyses involving the comparison of two groups. Paired student's *t* test was used to compare before and after applying NMDA. A one-way or two-way analysis of variance (ANOVA) with Bonferroni post hoc test was performed the comparison of three or more groups. In all cases, $p < 0.05$ was considered statistically significant.

Results

Distribution and morphology of 5-HT neurons in the MLR

Although the distribution of 5-HT neurons in the brain has been extensively studied, no research is focused on the distribution of 5-HT neurons in the MLR, and even if the existence of serotonin neurons in this region is controversial. In this study, we studied the distribution of 5-HT neurons in the MLR by using transgenic mice and immunofluorescence technology. Results showed that 5-HT neurons existed in the MLR, and differentially distributed across the rostro-caudal axis, densely concentrated in caudal PPN and extended dorsally into rostral cuneiform nucleus which could be seen in transverse slices (Fig. 1b, c) and sagittal slices (Fig. 1g). Immunofluorescent results confirmed that EYFP positive neurons in the MLR were THP2-expressed neurons (Fig. 1d1–d4), and these neurons existed in the region of PPN by staining ChAT (Fig. 1e, f). The number of 5-HT neurons in the MLR were estimated as 100–200 through analyzing the transverse and sagittal slices.

We studied morphology of 5-HT neurons through intracellular fluorescent dye of Dextran tetramethylrhodamine. Fluorescent images were analyzed using Sholl analysis technology. Figure 2a, b shows the process of Sholl analysis. Number of intersections, branch points, terminal points, diameter of soma, primary segments were used to describe the neuronal morphology in this study. Results showed that 100% 5-HT neurons ($n = 12$) in the MLR were multipolar neurons and could be divided into two types based on their dendritic morphology. One type was pyramidal neuron with conic shaped soma, a large apical dendrite (Fig. 2c, cell 1–3). Another type was stellate neuron with radial dendrites (Fig. 2c, cell 4–6). Statistical results indicated that number of intersections of stellate neurons were more than that of pyramidal neurons, especially in the range of 150–200 µm apart from soma (Fig. 2d, $p < 0.05$). The somatic diameter of two type neurons had no statistical difference (10–16 µm, Fig. 2e) but the branch points, terminal points, and primary segments of stellate neurons appeared to be bigger than those of pyramidal neurons (Fig. 2f, $p > 0.05$).

Figure 3 shows location and morphology of two type neurons in the PPN, where two pyramidal neurons (cell 1, 2 in Fig. 3b, c) and one stellate neuron (cell 3 in Fig. 3d) were labeled with intracellular tetramethylrhodamine (cells 1–3 in right side of Fig. 3a). These neurons were located in PPN with dendrites overlapped. Details of the morphology of the neurons showed that 5-HT neurons in the MLR were diversified. Stellate neurons might receive more information from neurons nearby the soma, whereas pyramidal neurons could communicate more with distant neurons. These results suggested that function of 5-HT neurons in the MLR might be different.

Different membrane properties between 5-HT and non-5-HT neurons

The passive membrane properties demonstrate the physical characteristics of the neurons such as the cell size and shape. Parameters E_m, C_m, R_{in}, and τ_m were used to describe the passive membrane properties. A total of 63 neurons (5-HT neurons = 35, non-5-HT neurons = 28) in the MLR were measured in this study. The E_m of 5-HT neurons were significantly more hyperpolarized than that of non-5-HT neurons by 4.2 ± 1.5 mV (5-HT neurons -69.2 ± 4.2, non-5-HT neurons -65.0 ± 1.9 mV, $p < 0.05$, Fig. 4a). 5-HT neurons had a very significantly smaller Rin compared to non-5-HT neurons by 711.1 ± 194.1 MΩ (5-HT neurons: 1410.1 ± 616.9 MΩ, non-5-HT neurons: 2121.2 ± 866.2 MΩ, $p < 0.01$, Fig. 4b). There was no significant difference in Cm between the 5-HT (36.4 ± 14.9 pF) and non-5-HT (31.9 ± 9.5 pF) neurons (Fig. 4c). The τ_m of 5-HT neurons were 14.4 ± 5.5 ms significantly smaller than that of non-5-HT neurons (5-HT neurons 49.7 ± 19.4 ms, non-5-HT neurons: 64.1 ± 24.6 ms, $p < 0.05$, Fig. 4d). The above results generally exhibited significant difference in passive membrane properties between the 5-HT and non-5-HT neurons, suggesting that 5-HT neurons in the MLR might be larger than non-5-HT neurons in terms of cell soma size, the number of dendrites, or potassium-meditated leak conductance which contributed to building of E_m (Fig. 4a).

The AP threshold, AP amplitude, AP half-width, Rheobase, AHP amplitude and AHP half-decay were used to describe the active membrane properties of neurons in this study. 5-HT neurons had a more depolarized AP threshold by 5.4 ± 1.9 mV compared to non-5-HT neurons (5-HT neurons -32.1 ± 7.4 mV, non-5-HT neurons -37.5 ± 7.8 mV, $p < 0.05$, Fig. 4e). No significant difference was found in AP amplitude (5-HT neurons 58.9 ± 12.8 mV, non-5-HT neurons 53.5 ± 10.3 mV, $p > 0.05$, Fig. 4f) and AP half-width (5-HT neurons 4.7 ± 1.1 ms, non-5-HT neurons 4.5 ± 1.6 ms, $p > 0.05$, Fig. 4g) between 5-HT and non-5-HT neurons. 5-HT neurons had a higher rheobase than non-5-HT neurons (5-HT neurons 21.3 ± 12.4 pA, non-5-HT neurons 12.3 ± 6.5 pA, $p < 0.01$, Fig. 4h). AHP amplitude of 5-HT neurons were 5.3 ± 2.0 mV bigger than that of non-5-HT neurons (5-HT neurons 23.6 ± 10.4 mV, non-5-HT neurons 18.3 ± 5.4 mV, $p < 0.05$, Fig. 4i). There was no significant difference in AHP half-decay between 5-HT and non-5-HT neurons (5-HT neurons 331.6 ± 157.7 ms, non-5-HT neurons: 300.0 ± 121.1 ms). These results indicated that the excitability of 5-HT neurons in the MLR was lower than that of non-5-HT neurons.

Different firing patterns and membrane properties of the 5-HT neurons

In this study, stable firings were evoked by injecting double amount of rheobase and 1.5-s step current into the 5-HT neurons ($n = 35$) in the MLR. These neurons could be divided

Fig. 2 Morphology of 5-HT neurons in the MLR. **a** An example of 5-HT neuron labeled by Fluorescent dye Dextran, tetramethylrhodamine. a1 An image of the same neuron which was merged by green and red fluorescent image. **b** Schematic diagram of the Sholl analysis to obtain the morphological parameters such as number of intersections, branch point, terminal points. **c** Representative reconstructions of fluorescent dye dextran-labeled neurons analyzed using Sholl analysis. 5-HT neurons could be divided into two types based on their morphology. Cell 1–3 with conic shaped soma, a large apical dendrite were classified into pyramidal neuron group. Neurons with radial dendrites were classified as stellate neuron group (cell 4–6). **d** Statistic result showed that intersections were obviously different between the two type neurons especially in the range of 150–200 µm ($p < 0.05$). **e** The soma of most neurons was oval. Statistic result showed that there was no difference in short or long diameter between two type neurons. **f** The number of branch points, terminal points, and primary segments of stellate neurons tended to be more than that of pyramidal neurons ($p > 0.05$). * Represented significant difference ($p < 0.05$)

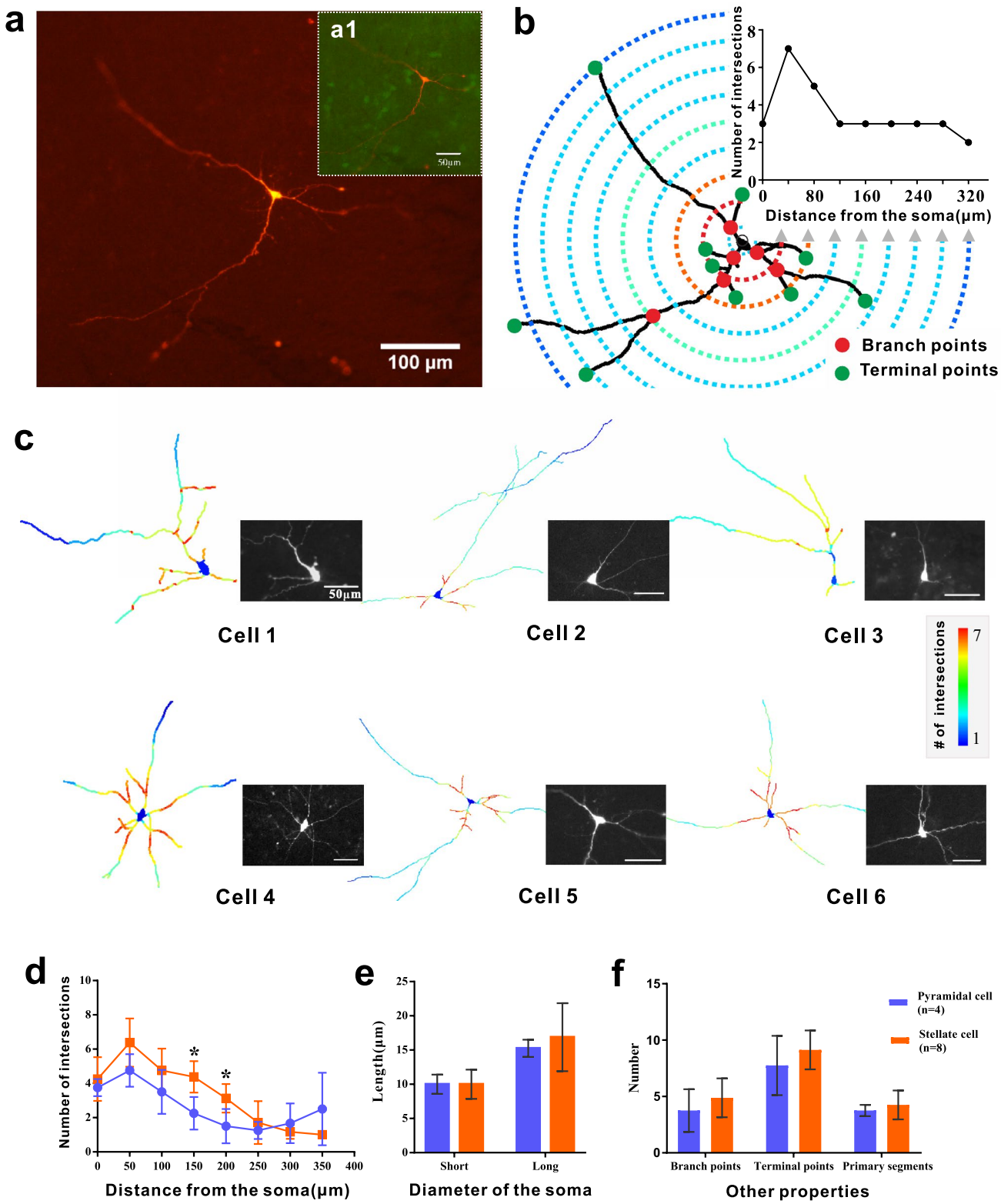
a
a1
50μm
100 μm
b
Number of intersections
Distance from the soma(μm)
Branch points
Terminal points
c
50μm
Cell 1
Cell 2
Cell 3
# of intersections
7
1
Cell 4
Cell 5
Cell 6
d
Number of intersections
Distance from the soma(μm)
e
Length(μm)
Short
Long
Diameter of the soma
f
Number
Pyramidal cell (n=4)
Stellate cell (n=8)
Branch points
Terminal points
Primary segments
Other properties

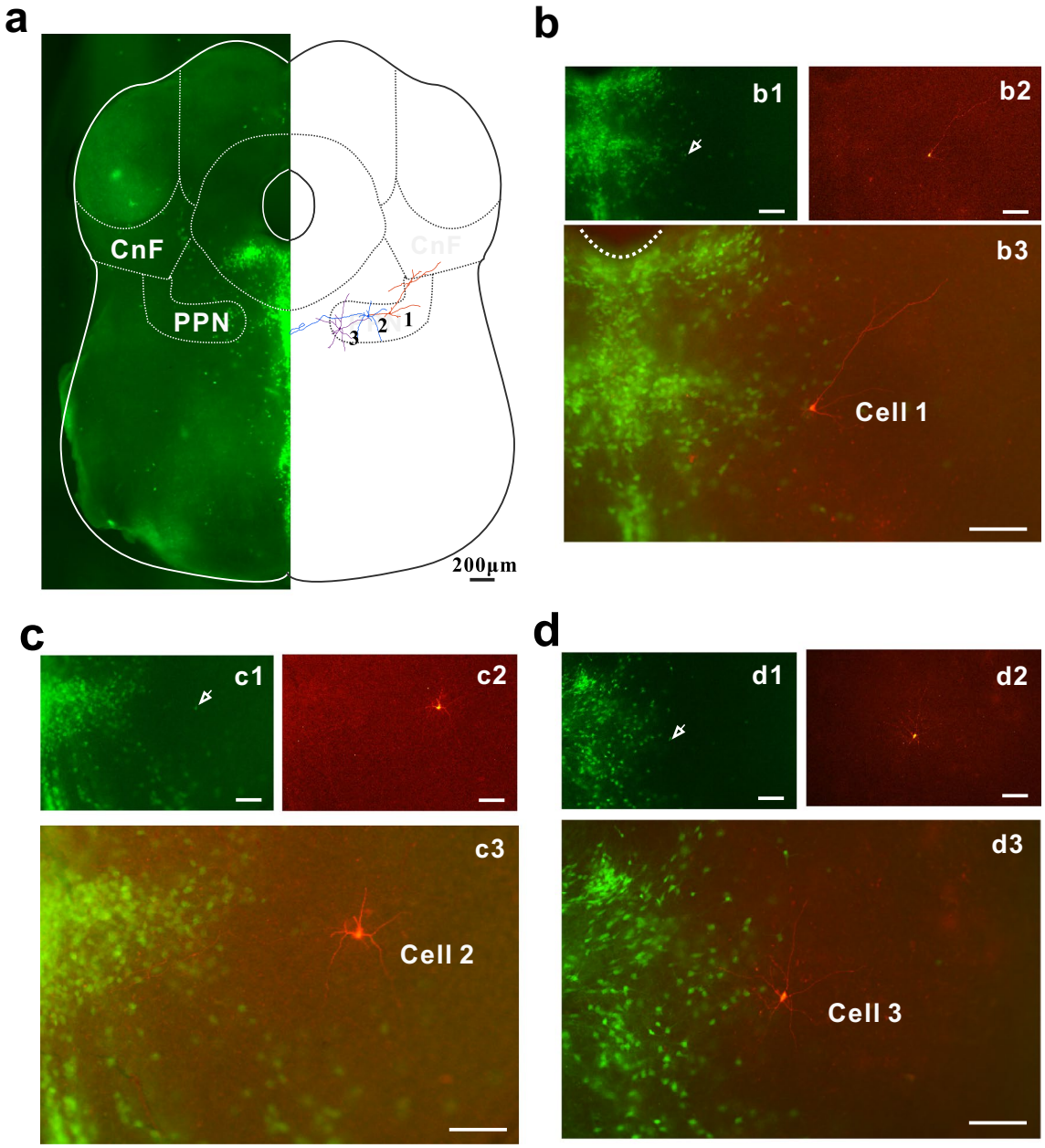

Fig. 3 Location and morphology of two type neurons. **a** A schematic view of the pyramidal neurons (cell 1, 2) and stellate neuron (cell 3) in the MLR. **b** Fluorescence images (b1, green; b2, red; and b3, merge) of a pyramidal neuron (cell 1) were collected. **c** Fluorescence images (c1, green; c2, red; c3, merge) of another pyramidal neuron (cell 2) were collected. **d** Fluorescence images (d1, green; d2, red, d3, merge) of a stellate neuron (cell 3) were collected

into three types with respect to their firing patterns. 11% of the neurons (4/35) were classified as single-spike type which generally elicited 1 or 2 spikes (Fig. 5a, top) and 31% as phasic-firing type (11/35) which discharged briefly at beginning of current injection and exhibited a spike frequency adaptation (Fig. 5a, middle-upper). The majority of neurons, 58% (20/35), fired repetitively over the entire current injection and were classified as tonic-firing type (Fig. 5a, middle-lower). Furthermore, the tonic-firing neurons could be further divided into two subtypes based on their variation of firing frequency. 40% (8/20) tonic-firing neurons displayed a spike frequency adaptation (Fig. 5b, top) and 60% (12/20) neurons fired with a steady frequency (Fig. 5b, middle).

Among these three type neurons, significant differences were found in some of their intrinsic membrane properties. The V_{th} of single-spike neurons (-21.1 ± 3.8 mV) was 11.4 ± 3.0 mV and 13.1 ± 3.6 mV more depolarized than that of phasic-firing (-32.5 ± 5.6 mV) and

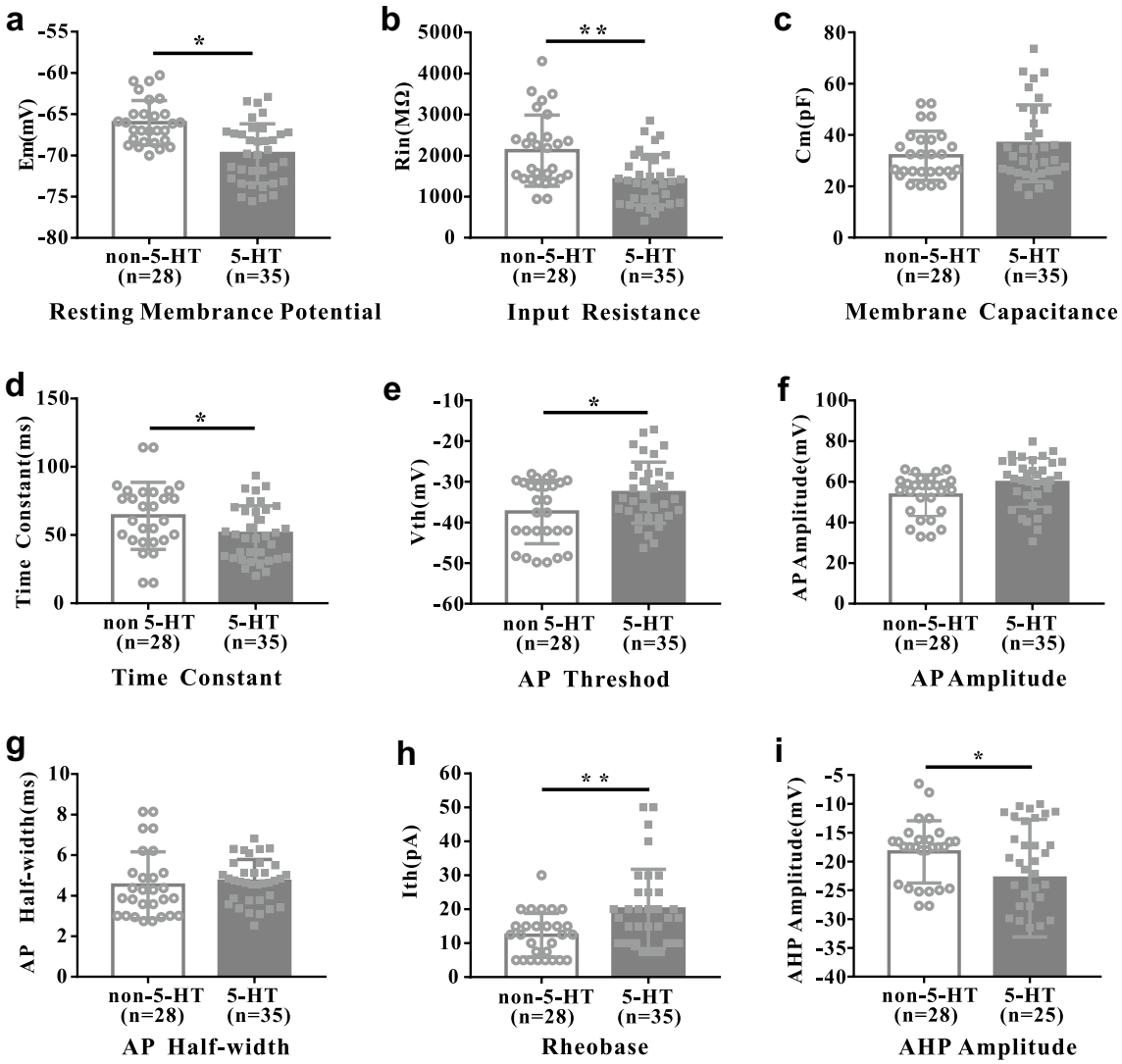

Fig. 4 The membrane properties of 5-HT ($n=35$) and non-5-HT ($n=28$) neurons in the MLR. **a** The Em of 5-HT neurons was more hyperpolarized than that of non-5-HT neurons ($p<0.05$). **b** The Rin of 5-HT neurons was smaller than that of non-5-HT neurons ($p<0.01$). **c** There was no significant difference in Cm between 5-HT and non-5-HT neurons. **d** The τ_m of 5-HT neurons was smaller than that of non-5-HT neurons ($p<0.05$). **e** The AP threshold of 5-HT neurons was more depolarized than that of non-5-HT neurons ($p<0.05$). No significant difference was found in AP amplitude (**f**) and AP half-width (**g**) between 5-HT and non-5-HT neurons ($p>0.05$). **h** 5-HT neurons had a higher rheobase than non-5-HT neurons ($p<0.01$). **i** The AHP amplitude of 5-HT neurons was bigger than that of non-5HT neurons ($p<0.05$). * represented significant difference ($p<0.05$), ** represented highly significant difference ($p<0.01$). The open circle represented the measured value of each non-5-HT neurons, and the solid square represented the measured value of each 5-HT neurons

tonic-firing neurons (-34.0 ± 7.0 mV), respectively ($p<0.05$, Fig. 5c). Tonic-firing neurons showed a 3.5 ± 2.3 mV and 3.1 ± 1.5 mV higher Em than other two type neurons, respectively (single spike -71.3 ± 3.3 mV; phasic -70.9 ± 3.3 mV; tonic -67.8 ± 4.4 mV, $p<0.05$, Fig. 5d). Except for the V_{th} and E_m, no significant difference was found in other membrane properties among the three type neurons. The detailed results are summarized in Table 1. These results showed that single-spike neurons had the lowest excitability among the three type neurons whereas the excitability of tonic-firing neurons were the highest.

H-current (Ih) is a nonselective cation current activated by hyperpolarization of membrane potential. The Ih-mediated depolarizing sag was examined in the present study. Our results showed that 20% 5-HT neurons (7/35) exhibited depolarizing sags which were triggered by hyperpolarizing step currents of − 10 pA and 1.5 s duration (Fig. 5e).

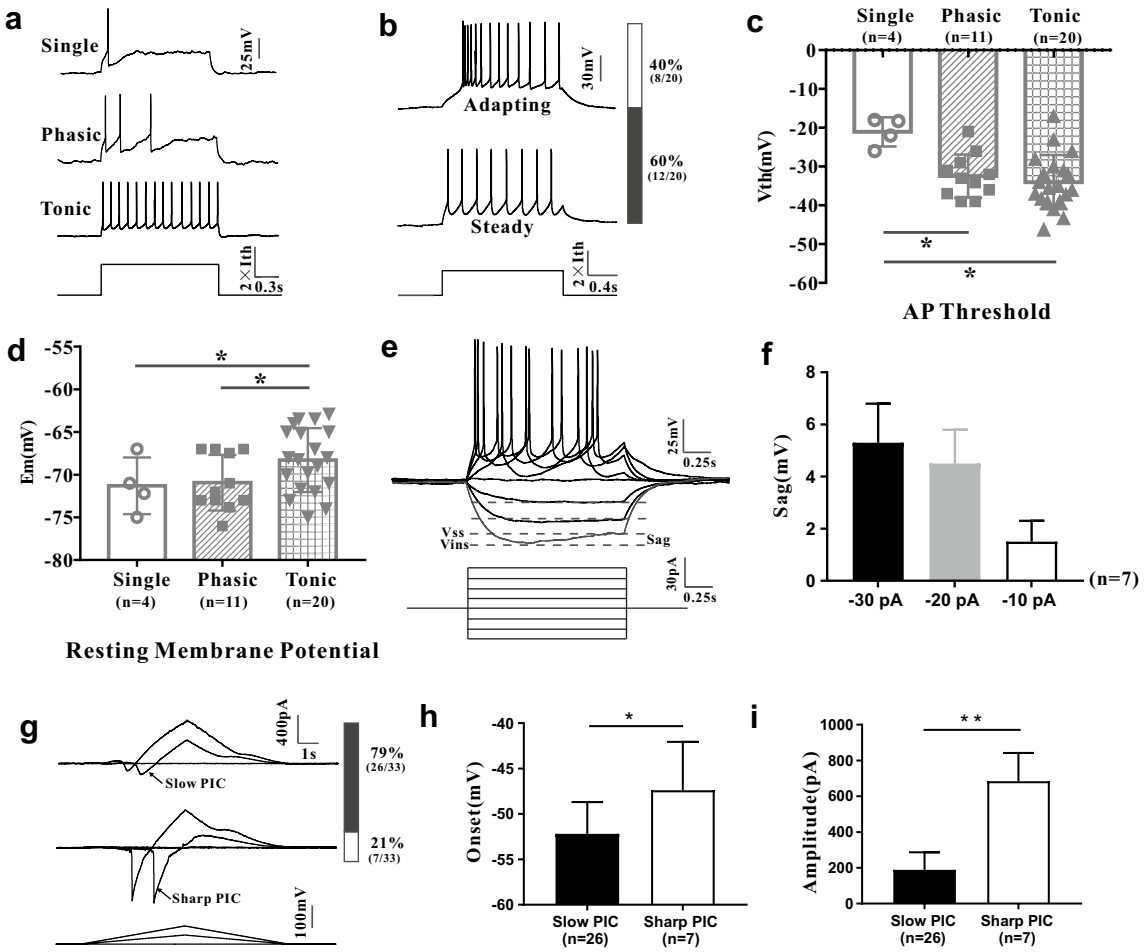

Fig. 5 Different firing patterns and membrane properties of the 5-HT neurons. **a** 1.5 s, double amount of rheobase current was injected into the neurons to evoke stable firing (**a**, bottom). 5-HT neurons could be divided into single spike, phasic-firing, and tonic-firing types based on firing patterns. Single-spike type neurons generated only 1 or 2 spikes during the current stimulation (**a**, top). Phasic-firing neurons fired at the beginning period of current injection, and then had obvious spike frequency attenuation (**a**, middle-upper). Continuous firings were recorded in tonic-firing neurons over the entire current injection (**a**, lower-middle). b: Examples of two subtypes in tonic-firing neurons. One subtype displayed a spike frequency adaptation (top), and another subtype fired with a steady frequency (bottom). The bar indicated the ratio of the two type neurons, and the white part represented the adapting type and the grey part represented the steady type. **c** Statistic results showed that single-spike neurons had a more depolarized V_{th} than phasic and tonic-firing neurons ($p<0.05$). **d** The Em of tonic-firing neurons was more depolarized than that of other two type neurons ($p<0.05$). **e** Hyperpolarizing current (1.5 s, −40 pA, −30 pA) could trigger H-current-mediated depolarizing sags. **f** Statistic result showed that H-current-mediated depolarizing sags, triggered by hyperpolarizing step currents of −10 pA and 1.5 s duration, were shown as current-dependent ($n=7$). **g** Two type persistent inward currents (PICs) were observed in 5-HT neurons. One type had a slow-shape shown as **g** (top), and another type had a sharp-shape (**g**, middle). The bar indicated the ratio of the two type PICs. **h** Onset of slow-PIC was significantly hyperpolarized that sharp PIC. **i** Amplitude of the slow-PIC was very smaller than sharp PIC ($p<0.01$). *Represented significant difference ($p<0.05$). ** Represented very significant difference ($p<0.01$). The open circle represented single-spike neurons; solid square: phasic-firing neurons; and solid triangle: tonic-firing neurons

The amplitude of Ih-mediated sags were shown as current-dependent with mean amplitude ranging from 1.8 (elicited by the −10 pA step) to 5.4 mV (elicited by the −30 pA step) ($n=7$, Fig. 5f). In fact, the injected step currents determined the extent of hyperpolarization of membrane potential which determined the amplitude of the sags. In the present study, the persistent inward currents (PICs) were also examined in 35 5-HT neurons in the MLR. PICs were observed in 95% 5-HT neurons. Moreover, the PICs could be divided into slow-PIC (26/33, Fig. 5g, top) and sharp-PIC (7/33, Fig. 5g, middle) types. The PIC onset of slow-PIC type neurons were significantly lower than that of sharp-PIC type neurons by 4.8 ± 2.0 mV (slow-PIC type −52.2 ± 1.0 mV, sharp-PIC type −47.4 ± 2.0 mV, $p<0.05$, Fig. 5h). The PIC amplitude of slow-PIC type neurons were much smaller than that of sharp-PIC type neurons by

Table 1 Membrane properties of 5-HT neurons classified in cell types

	Single spike (*S*, $n=4$)	Phasic firing (*P*, $n=11$)	Tonic firing (*T*, $n=20$)	*S* vs *P*	*S* vs *T*	*P* vs *T*
E_m, mV	−71.3 ± 3.3	−70.9 ± 3.3	−67.8 ± 4.4	NS	*	*
R_{in}, MΩ	1457.5 ± 893.8	1392.1 ± 582.4	1410.5 ± 612.9	NS	NS	NS
C_m, pF	31.0 ± 4.1	40.1 ± 15.2	35.5 ± 16.1	NS	NS	NS
τ_m, ms	53.5 ± 9.8	51.9 ± 18.9	47.7 ± 21.4	NS	NS	NS
V_{th}, mV	−21.1 ± 3.8	−32.5 ± 5.6	−34.0 ± 7.0	*	*	NS
Rheobase, pA	30.8 ± 20.6	23.4 ± 14.8	18.3 ± 7.8	NS	NS	NS
AP amplitude, mV	51.4 ± 15.0	61.0 ± 10.1	59.3 ± 13.8	NS	NS	NS
AP half-width, ms	5.1 ± 1.3	5.0 ± 0.9	4.4 ± 1.1	NS	NS	NS
AHP amplitude, mV	33.4 ± 5.2	21.8 ± 10.1	22.7 ± 10.6	NS	NS	NS
AHP 1/2 decay, ms	384.4 ± 72.3	301.1 ± 215.2	337.9 ± 134.8	NS	NS	NS

*Significant difference with $p<0.05$

NS not significant difference

495.1 ± 56.9 pA (slow-PIC type 188.9 ± 27.2 pA, sharp-PIC type 684.0 ± 59.7 pA, $p<0.01$, Fig. 5i). All these results indicated that 5-HT neurons in the MLR displayed diverse firing patterns and membrane properties. The diversity of 5-HT neurons in the MLR provided potential insight into the cellular basis for multifunctional control in this region.

Effects of NMDA on the 5-HT neurons

NMDA modulation of 5-HT neurons in MLR was investigated in this study. Three types of 5-HT neurons were recorded with bath application of 10–15 μM NMDA. The effects of NMDA on these neurons are summarized in Table 2 and illustrated in Fig. 6. As shown in Fig. 6a, NMDA induced an obvious depolarization (~ 10 mV) of resting membrane potential. These changes could be recovered through washout (15–20 min). Since the single-firing neurons accounted for a small proportion ($n=2$) of the total neurons recorded with NMDA ($n=20$), the statistical results were mainly focused on phasic and tonic-firing neurons. Statistical analysis showed that NMDA induced significant depolarization of the resting membrane potential ($p<0.05$, Fig. 6b) and hyperpolarization of V_{th} ($p<0.05$, Fig. 6d) in tonic-firing neurons. A typical example is shown in Fig. 6c, where a 10 μM NMDA induced a 4.5 mV hyperpolarization of V_{th} in a tonic-firing neuron. We examined the relation of firing frequency and injected current (*F–I* relation) in phasic and tonic-firing neurons in the present study. NMDA generally shifted the *F–I* curve to the left and reduced the *F–I* slope (Fig. 6e). Statistical results showed that the main effects of NMDA on *F–I* relation were to shift the *F–I* curve to the left ($p<0.05$, $n=8$, Fig. 6f) with a small decrease in slope ($p>0.05$, Fig. 6g). The effect of NMDA on AHP was investigated in the present study. Our data showed that NMDA could

Table 2 The effects of NMDA on 5-HT neurons

	Single ($n=2$) control	Single (change) NMDA	Phasic ($n=6$) control	Phasic (change) NMDA	Tonic ($n=12$) control	Tonic (change) NMDA
E_m, mV	−69.6 ± 3.7	5.1 ± 3.9	−69.7 ± 4.1	5.1 ± 2.3	−68.5 ± 4.6	4.9 ± 1.8*
R_{in}, MΩ	1409.5 ± 19.1	−61.0 ± 226.0	1162.3 ± 227.1	−119.4 ± 87.3	1533.9 ± 686.2	−133.2 ± 164.8
C_m, pF	33.4 ± 3.7	−0.4 ± 8.6	46.9 ± 9.6	−11.4 ± 4.7	35.6 ± 12.6	−1.5 ± 3.0
τ_m, ms	46.9 ± 4.3	−3.5 ± 4.5	52.2 ± 15.5	−15.2 ± 2.6	49.9 ± 24.8	7.5 ± 22.2
V_{th}, mV	−18.1 ± 0.1	3.5 ± 4.6	−30.0 ± 6.5	−1.5 ± 1.1	−33.9 ± 5.3	−3.2 ± 1.0*
Rheobase, pA	39.0 ± 29.7	10.0 ± 10.0	29.2 ± 14.6	−4.1 ± 2.3	18.8 ± 8.6	−5.6 ± 3.4
AP amplitude, mV	42.3 ± 16.0	−0.9 ± 12.9	62.0 ± 7.7	−5.0 ± 3.8	59.9 ± 13.5	−2.1 ± 3.9
AP half-width, ms	4.8 ± 0.4	−0.5 ± 0.5	4.1 ± 0.9	−0.3 ± 0.3	4.5 ± 1.3	−0.1 ± 0.2
AHP amplitude, mV	30.2 ± 0.3	−1.6 ± 0.6	23.1 ± 13.5	−3.2 ± 1.7	23.2 ± 10.0	−1.8 ± 1.0
AHP 1/2 decay, ms	333.7 ± 15.2	−210.2 ± 69.2	370.6 ± 109.9	−61.8 ± 26.5	339.5 ± 125.4	−58.3 ± 13.8*

*Significant difference with $p<0.05$

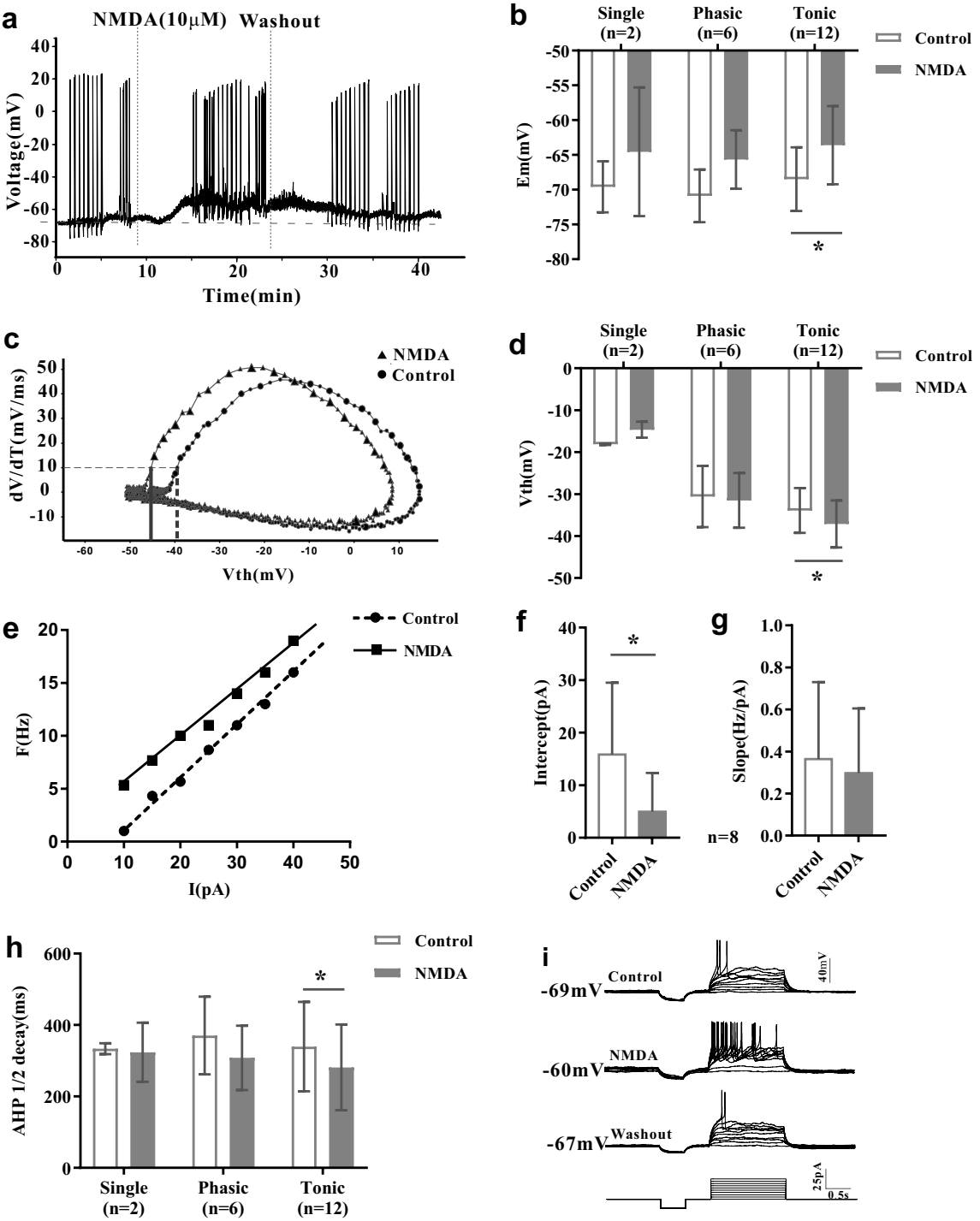

Fig. 6 Effects of NMDA on the 5-HT neurons. **a** Continuous record displayed that 10 μM NMDA induced ~ 10 mV depolarization of the resting membrane potential. This change could be recovered through washout (15–20 min). **b** Paired *t* test statistic results showed that 10–15 μM NMDA induced significant depolarization of resting membrane potential in tonic-firing neurons ($n=12$) ($p<0.05$). **c** A typical example showed that NMDA induced hyperpolarization of V_{th} in a tonic-firing neuron. **d** The V_{th} of tonic-firing neurons was significantly hyperpolarized by NMDA ($p<0.05$). **e** An example of tonic-firing neuron that NMDA shifted the *F–I* curve to the left and reduced the slope. **f** The statistic results showed that NMDA significantly reduced the intercept between the *F–I* curve and the *x* axis (ΔI, $n=8$, $p<0.05$). g NMDA tended to reduce the slope of *F–I* curve ($n=8$, $p>0.05$). **h** AHP half-decay in tonic-firing neurons significantly decreased after application of NMDA ($p<0.05$). **i** The firing pattern of one 5-HT neuron was changed from single-spike pattern to phasic-firing pattern by NMDA. The effect of NMDA on firing pattern of this neuron was washable after 15-min washout

produce significant reduction of AHP half-decay in tonic-firing neurons ($p < 0.05$, Fig. 6h). Except for Em, Vth and AHP half-decay, NMDA did not produce any significant change in other membrane properties of 5-HT neurons in the MLR (Table 2). NMDA-induced alteration of firing pattern was observed in our experiments. An example is shown in Fig. 6i, where NMDA changed a single-spike 5-HT neuron to phasic-firing neuron accompanied by a 9 mV depolarization of E_m. The effect of NMDA on firing pattern in this neuron was washable after 15-min washout.

All these results demonstrated that NMDA increased the neuronal excitability and enhanced the output of 5-HT neurons via hyperpolarizing V_{th}, reducing AHP half-decay and shifting *F–I* curve to the left. Furthermore, the excitatory effects of NMDA on 5-HT neurons were shown to be dependent on the firing pattern of the neurons. In general, tonic-firing neurons appeared to be more sensitive to NMDA in terms of hyperpolarization of V_{th} and reduction of AHP half-decay, suggesting that tonic-firing neurons might play a key role in mediating modulation of NMDA in the MLR.

Discussion

Since Shik and colleagues discovered that electrical stimulation of the MLR could induce locomotion in decerebrate cats in 1966 (Shik et al. 1966), the MLR has been considered as a crucial region for initiation and control of locomotion via descending pathways (Noga et al. 1995). These pathways start from the MLR, bilaterally descend to reticulospinal neurons of the pons and medulla (Steeves and Jordan 1984; Ryczko et al. 2016; Takakusaki et al. 2016; Brownstone and Chopek 2018), and then go through the ventral funiculus (Noga et al. 2003) to activate the CPGs for control of locomotion. However, the cellular and molecular pathways remain unclear, and in particular, the distribution and intrinsic membrane properties of 5-HT neurons in the MLR. Using transgenic ePet-EYFP mice and immunofluorescence we confirmed that 5-HT neurons sparsely distributed in the MLR, and for the first time we investigated the electrophysiological and NMDA-modulatory properties of these 5-HT neurons. Also, we made a comparison of membrane properties between the 5-HT and non-5-HT neurons in the MLR and found that the 5-HT and non-5-HT neurons were significantly different in both passive and active membrane properties. NMDA enhanced the excitability of 5-HT neurons and this enhancement of excitability depended on the firing patterns of the neurons. This study formed a basis for further study of functional roles of the MLR in initiating and controlling locomotion.

Existence of 5-HT neurons in the MLR

Serotonin (5-HT), a major neuromodulator in the nerve system, is released from serotonergic neurons that largely concentrate in midline of brainstem. The detailed distribution and connectivity of the 5-HT neurons have been well studied via using histofluorescence technique (Dahlstroem and Fuxe 1964), immunohistochemical method (Takeuchi et al. 1982; VanderHorst and Ulfhake 2006), and rabies virus tracing approaches (Ogawa Sachie et al. 2014). The majority of serotonin neurons (75%) are located within raphe nucleus (Wiklund et al. 1981), which can be divided into nine groups (B1–B9) (Dahlstroem and Fuxe 1964). 5-HT neurons in the dorsal raphe nucleus (B6, B7) and median raphe nucleus (B8) have extensive afferent and efferent connections to other regions of brain and contribute to generation of various behaviors such as reward, sleep–wake cycle, major depression, and movement disorders (Kawashima 2018). 5-HT neurons in raphe pallidus (B1), raphe obscurus (B2) and raphe magnus (B3) are involved in motor control (Schmidt and Jordan 2000; Jordan and Slawinska 2011). Previous studies mainly focused on these 75% of 5-HT neurons which distribute in raphe nucleus, and little is known about the other 25% of the 5-HT neurons which are located outside of the raphe nucleus in brainstem (Wiklund et al. 1981). Distribution, morphology and function of these neurons are rarely studied. Because these neurons are adjacent to the raphe nucleus, they are thought to belong to the latter. But some studies indicate that 5-HT neurons are heterogeneous in central nervous system and that the physiologic and functional properties of 5-HT neurons in raphe nucleus are different (Abrams et al. 2004). The cuneiform nucleus (CnF) and the pedunculopontine nucleus (PPN), adjacent to dorsal raphe nucleus and median raphe nucleus, are two core components of the MLR. It has been a controversial issue whether 5-HT neurons exist in the MLR. Pose and coworkers reported that cuneiform nucleus (CnF) did not contain serotonergic neurons in cat (Pose et al. 2000). However, Beitz discovered that 5-HT neurons existed in cuneiform nucleus (CnF) and projected to nucleus raphe magnus in rat (Beitz 1982). In this study, we hypothesized that 5-HT neurons exist in the MLR in neonatal rodents. To address this issue, we used ePet-EYFP mice in which the ePet-driven yellow fluorescent protein was expressed specifically in 5-HT neurons (Scott et al. 2005; Hawthorne et al. 2010) to visually analyze the qualitative and quantitative distribution of 5-HT neurons in the MLR. Our results showed that 5-HT neurons dispersedly distributed in the MLR, especially in caudal-ventral PPN in transverse slices. Interestingly, 5-HT neurons were differentially distributed across the rostro-caudal axis from a sagittal perspective, and densely concentrated in caudal PPN and extend dorsally into rostral cuneiform nucleus, similar to the distribution of glutamatergic neuron in PPN

(Mena-Segovia and Bolam 2017). Similar results were obtained in Calizo and coworkers study, in which glutamate neurons were intermixed and co-localized with 5-HT neurons within raphe subfields (Calizo et al. 2011). In an earlier study it was shown that cultured rat mesopontine serotonergic neurons co-released serotonin and glutamate (Johnson 1994). These results demonstrated that 5-HT neurons exist in the MLR, and there is a relationship between serotonergic neurons and glutamatergic neurons. In order to confirm that the EYFP positive neurons are serotonergic neurons, we did extra experiments for staining of tryptophan hydroxylase 2 (TPH2), the main marker of 5-HT neurons, in EYFP positive neurons. The immunofluorescence results confirmed that EYFP positive neurons in PPN were THP2 positive neurons and thus verified the reliability of ePet-EYFP transgenic mice for study of 5-HT neurons in midbrain (Fig. 1d1–d4). Furthermore, we defined the borders of the PPN by staining for choline acetyltransferase (ChAT) and confirm the existence of 5-HT neurons in the PPN (Fig. 1e, f). In summary, we confirmed the existence of 5-HT neurons in the MLR in neonatal mice and solved this controversial issue which might be related to the different methods, species or the age of the animals.

Neuronal heterogeneity in the MLR

The mesencephalic locomotor region (MLR), a brainstem structure capable of modulating locomotion, has been studied extensively over past decades. Results from numerous studies show that MLR is mainly composed of the pedunculopontine nucleus (PPN) and the cuneiform nucleus (CnF). The MLR controls locomotor activity through descending pathways from MLR to medullary reticular formation and spinal cord. The MLR also receives a wide range of innervations from cerebellum, motor cortex, basal ganglia and hypothalamus, and adjusts motor commands to adapt to different behavioral circumstances such as exploratory, appetitive, and defensive behaviors (Jordan 1998; Jordan et al. 2008). In addition to motor control, MLR performs important roles in many other functional behaviors such as sleep, attention, and emotion (Ros et al. 2010). Multiple functions predict the neuronal heterogeneity in the MLR. However, the neuronal populations and circuit organizations that underlie such complicated functions remain unclear. In this study, we verified the existence of 5-HT neurons in MLR and for the first time we investigated the electrophysiological and morphological properties of these neurons and explored difference in both passive and active membrane properties between 5-HT and adjacent non-5-HT neurons in the MLR. We further reported that 5-HT neurons in MLR could be divided into three subtypes, similar to the results from recent study of 5-HT neurons in brainstem (Dai et al. 2016).

Differences in membrane properties between 5-HT and non-5-HT neurons in the raphe nucleus, a nucleus adjacent to the MLR, have been reported in previous studies (Calizo et al. 2011). Our results were consistent with these studies and indicated that the excitability of 5-HT neurons was lower than that of non-5-HT neurons in the MLR, suggesting that 5-HT neurons would be less responsive to excitatory input than non-5-HT neurons. Immunohistochemical data showed that these adjacent non 5-HT neurons in MLR were potential candidate for glutamatergic and GABAergic neurons (Calizo et al. 2011) and might be more excitable than 5-HT neurons in the same region. In fact, moderate release of 5-HT was sufficient to modulate locomotion and enhance the excitability of motoneurons by activating 5-HT2 receptors, while stronger release inhibited locomotion and motoneuron excitability due to activating extra synaptic 5-HT1A receptors, which secured rotation of motor units (Cotel et al. 2013; Perrier and Cotel 2015). These results provided evidence that serotonergic system could perform broader dynamic function in modulating locomotion.

In addition to the three firing patterns, the Ih (shown as depolarizing sag) and PIC were also observed in 5-HT neurons. The PIC was shown as multiple patterns (sharp- and slow-PIC) in 5-HT neurons in the MLR, similar to the report in spinal interneurons (Dai and Jordan 2010a, 2011). The Ih and PIC are two ionic currents playing crucial, multifunctional roles in generating locomotion (Kjaerulff and Kiehn 2001; Powers and Binder 2003; Robinson and Siegelbaum 2003; Heckman et al. 2008) and can be enhanced by 5-HT (Dai and Jordan 2010b). The expression of Ih and PIC in 5-HT neurons in the MLR suggested that multiple channels could contribute to regulation of excitability and output of the 5-HT neurons. Our findings implicated that the MLR was composed of heterogeneous neurons and that the diversity in discharge patterns of 5-HT neurons could provide nervous system with more dynamic properties for performing multi-functions in the MLR.

NMDA increased the excitability of the 5-HT in the MLR

It was shown in early studies that NMDA alone could initiate locomotion in vitro (Kudo and Yamada 1987) and in vivo preparations (Takakusaki et al. 2003). With advances in mouse genetics, optogenetics and viral tools it becomes easier for us to manipulate discrete groups of neurons in mice and investigate their functions in motor control. Results from a series of studies indicated that glutamatergic neurons in MLR (Roseberry et al. 2016; Caggiano et al. 2018; Josset et al. 2018b) and the lateral paragigantocellular nucleus (LPGi) (Capelli et al. 2017) were essential to speed and gait selection. However, combination of NMDA and 5-HT could induce more robust fictive locomotion than NMDA alone

(Whelan et al. 2000). NMDA-induced locomotion could be blocked by serotonin receptor antagonist (MacLean et al. 1998) and the voltage-sensitivity of NMDA receptor on motoneurons could be modulated by 5-HT (MacLean and Schmidt 2001). These results indicated interaction between glutamatergic and serotonergic modulations in motor system. However, the cellular basis for this interaction is unclear. In this study, we investigated NMDA modulation of 5-HT neurons in the MLR. Glutamate receptors (NMDA, AMPA, and kainite receptors) were important for rhythmic generation in mammalian spinal motor system (Kiehn et al. 2008), while 5-HT also play an essential role in controlling rhythmicity (Dai and Jordan 2010b), oscillatory behavior (Carlin et al. 2006), and coordination of locomotion (Noga et al. 2009). Our results showed that NMDA increased the excitability of 5-HT neurons. This interaction between 5-HT neurons and NMDA modulation included membrane oscillation, Vth hyperpolarization, lowering of rheobase, reduction of AHP half-decay and left-shift of F-I relation. Similar changes in membrane properties had been reported in spinal neurons during fictive locomotion (Brownstone et al. 1992; Dai et al. 2002, 2018) or in neuromodulations (Fedirchuk and Dai 2004; Dai et al. 2009b). The current studies mainly focus on the role of co-application of NMDA and 5-HT in the producing locomotor-like activity in the spinal cord. However, recent evidence shows that the 5-HT neurons of nucleus raphe magnus (RMg) and the parapyramidal region (PPR) of the medulla are activated when locomotion is initiated by MLR stimulation (Noga et al. 2017b). Recent studies have identified glutamatergic neurons in the mesencephalic locomotor region–medulla pathway that initiate and accelerate locomotion (Yoo et al. 2017; Caggiano et al. 2018; Josset et al. 2018a). These results suggested that glutamatergic neurons may play a role in release of 5-HT in the spinal cord during locomotion. In addition, by perfusion of calcium-free aCSF, we confirmed that NMDA acted directly on the NMDA receptor on 5-HT neurons (data not shown). Serotonergic neurons in the dorsal raphe nucleus (DRN) of mice received monosynaptic functional glutamatergic input (Zhou et al. 2017). Optogenetic activation of DRN 5-HT neurons rapidly suppressed locomotion speed (Correia et al. 2017). These results showed that there was an interaction between serotonin neurons and glutamate neurons in brainstem. Therefore, our results suggested that NMDA might indirectly regulate rhythmic behavior via activation of 5-HT neurons in the MLR.

In this study we did not examine the mechanisms responsible for the increase in excitability after adding NMDA. However, our previous modeling study demonstrated that modulation of transient sodium current and/or delayed-rectifier potassium current could hyperpolarize the V_{th} (Dai et al. 2002) and that reduction of AHP current could induce the reduction of AHP half-decay (Dai et al. 2018). Therefore, modulation of transient sodium current, delayed-rectifier potassium current or calcium-dependent potassium SK current could be the potential cellular mechanisms underlying the increase in excitability seen on adding NMDA. A further study is required to address these issues.

Conclusions

Using ePet-EYFP transgenic mice and immunofluorescence technique, we demonstrated that 5-HT neurons sparsely distributed in the MLR, the pedunculopontine nucleus in particular. Furthermore, we revealed the unique membrane properties of 5-HT neurons in the MLR, which were different from those of non-5-HT neurons in the same region. Characterization of 5-HT and non-5-HT neurons in the MLR provided insights into the cellular basis for multifunctional roles of the MLR in initiating locomotion. NMDA increased excitability of the 5-HT neurons especially tonic-firing 5-HT neurons in the MLR, suggesting that the serotoninergic and glutamatergic systems could interact with each other in the MLR for generation and control of locomotion.

Acknowledgements This study was funded by National Natural Science Foundation of China (NSFC) to Yue Dai (31571222) and ECNU Academic Innovation Promotion Program for Excellent Doctoral Students to Renkai Ge (YBNLTS2019-029). The authors thank ECNU Multifunctional Platform for Innovation (011) for animal mold breeding.

Compliance with ethical standards

Conflict of interest The authors declare that they have no conflict of interest.

Ethical approval All applicable international, national, and/or institutional guidelines for the care and use of animals were followed. The animal protocols were reviewed and approved by the East China Normal University Laboratory Animal Center and Animal Experiment Ethics Committee.

References

Abrams JK, Johnson PL, Hollis JH, Lowry CA (2004) Anatomic and functional topography of the dorsal raphe nucleus. Ann N Y Acad Sci 1018:46–57. https://doi.org/10.1196/annals.1296.005

Beitz AJ (1982) The sites of origin brain stem neurotensin and serotonin projections to the rodent nucleus raphe magnus. J Neurosci 2:829–842. https://doi.org/10.1523/JNEUROSCI.02-07-00829.1982

Bowker RM, Westlund KN, Coulter JD (1981) Serotonergic projections to the spinal cord from the midbrain in the rat: an immunocytochemical and retrograde transport study. Neurosci Lett 24:221–226. https://doi.org/10.1016/0304-3940(81)90160-9

Brownstone RM, Chopek JW (2018) Reticulospinal systems for tuning motor commands. Front Neural Circuits 12:30. https://doi.org/10.3389/fncir.2018.00030

Brownstone RM, Jordan LM, Kriellaars DJ, Noga BR, Shefchyk SJ (1992) On the regulation of repetitive firing in lumbar motoneurones during fictive locomotion in the cat. Exp Brain Res 90:441–455. https://doi.org/10.1007/BF00230927

Caggiano V, Leiras R, Goni-Erro H et al (2018) Midbrain circuits that set locomotor speed and gait selection. Nature 553:455–460. https://doi.org/10.1038/nature25448

Calizo LH, Ma X, Pan Y, Lemos J, Craige C, Heemstra L, Beck SG (2011) Raphe serotonin neurons are not homogenous: electrophysiological, morphological and neurochemical evidence. Neuropharmacology 61:524–543. https://doi.org/10.1016/j.neuropharm.2011.04.008

Capelli P, Pivetta C, Esposito MS, Arber S (2017) Locomotor speed control circuits in the caudal brainstem. Nature 551:373–377. https://doi.org/10.1038/nature24064

Carlin KP, Dai Y, Jordan LM (2006) Cholinergic and serotonergic excitation of ascending commissural neurons in the thoraco-lumbar spinal cord of the neonatal mouse. J Neurophysiol 95:1278–1284. https://doi.org/10.1152/jn.00963.2005

Cheng Y, Ge RK, Chen K, Dai Y (2019) Modulation of NMDA-mediated intrinsic membrane properties of ascending commissural interneurons in neonatal rat spinal cord. J Integr Neurosci 18:163–172. https://doi.org/10.31083/j.jin.2019.02.129

Correia PA, Lottem E, Banerjee D, Machado AS, Carey MR, Mainen ZF (2017) Transient inhibition and long-term facilitation of locomotion by phasic optogenetic activation of serotonin neurons. eLife. https://doi.org/10.7554/eLife.20975

Cotel F, Exley R, Cragg SJ, Perrier JF (2013) Serotonin spillover onto the axon initial segment of motoneurons induces central fatigue by inhibiting action potential initiation. Proc Natl Acad Sci USA 110:4774–4779. https://doi.org/10.1073/pnas.1216150110

Dahlstroem A, Fuxe K (1964) Evidence for the existence of monoamine-containing neurons in the central nervous system. I. Demonstration of monoamines in the cell bodies of brain stem neurons. Acta Physiol Scand Suppl 232:231–255. https://doi.org/10.1111/j.1748-1716.1964.tb04017.x

Dai Y, Jordan LM (2010a) Multiple effects of serotonin and acetylcholine on hyperpolarization-activated inward current in locomotor activity-related neurons in Cfos-EGFP mice. J Neurophysiol 104:366–381. https://doi.org/10.1152/jn.01110.2009

Dai Y, Jordan LM (2010b) Multiple patterns and components of persistent inward current with serotonergic modulation in locomotor activity-related neurons in Cfos-EGFP mice. J Neurophysiol 103:1712–1727. https://doi.org/10.1152/jn.01111.2009

Dai Y, Jordan LM (2011) Tetrodotoxin-, dihydropyridine-, and riluzole-resistant persistent inward current: novel sodium channels in rodent spinal neurons. J Neurophysiol 106:1322–1340. https://doi.org/10.1152/jn.00918.2010

Dai Y, Jones KE, Fedirchuk B, McCrea DA, Jordan LM (2002) A modelling study of locomotion-induced hyperpolarization of voltage threshold in cat lumbar motoneurones. J Physiol Lond 544:521–536. https://doi.org/10.1113/jphysiol.2002.026005

Dai Y, Carlin KP, Li Z, McMahon DG, Brownstone RM, Jordan LM (2009a) Electrophysiological and pharmacological properties of locomotor activity-related neurons in cfos-EGFP mice. J Neurophysiol 102:3365–3383. https://doi.org/10.1152/jn.00265.2009

Dai Y, Jordan LM, Fedirchuk B (2009b) Modulation of transient and persistent inward currents by activation of protein kinase C in spinal ventral neurons of the neonatal rat. J Neurophysiol 101:112–128. https://doi.org/10.1152/jn.01373.2007

Dai Y, Yang SK, Chen K, Ge RK, Cheng Y, Song N, Ge X (2016) Characterization of serotonergic neurons in the medulla of ePet-EYFP Mice. SfN Abs:687.610

Dai Y, Cheng Y, Fedirchuk B, Jordan LM, Chu J (2018) Motoneuron output regulated by ionic channels: a modelling study of motoneuron frequency-current relationships during fictive locomotion. J Neurophysiol 120:1840–1858. https://doi.org/10.1152/jn.00068.2018

Fedirchuk B, Dai Y (2004) Monoamines increase the excitability of spinal neurones in the neonatal rat by hyperpolarizing the threshold for action potential production. J Physiol Lond 557:355–361. https://doi.org/10.1113/jphysiol.2004.064022

Ford B, Holmes CJ, Mainville L, Jones BE (1995) GABAergic neurons in the rat pontomesencephalic tegmentum: codistribution with cholinergic and other tegmental neurons projecting to the posterior lateral hypothalamus. J Comp Neurol 363:177–196. https://doi.org/10.1002/cne.903630203

Garcia-Rill E, Skinner RD, Fitzgerald JA (1985) Chemical activation of the mesencephalic locomotor region. Brain Res 330:43–54. https://doi.org/10.1016/0006-8993(85)90006-x

Ge RK, Cheng Y, Yang SK, Chen K, Song N, Ge X, Dai Y (2017) Electrophysiological and NMDA modulatory properties of neurons in the mesencephalic locomotor region of ePet-EYFP neonatal mice. CNS:P-216

George Paxinos KF, Paxinos George, Franklin Keith (2014) The mouse brain in stereotaxic coordinates. Academic, London

Grillner S, El Manira A (2015) The intrinsic operation of the networks that make us locomote. Curr Opin Neurobiol 31:244–249. https://doi.org/10.1016/j.conb.2015.01.003

Grillner S, Robertson B (2016) The Basal Ganglia over 500 million years. Curr Biol 26:R1088–R1100. https://doi.org/10.1016/j.cub.2016.06.041

Grillner S, McClellan A, Sigvardt K, Wallen P, Wilen M (1981) Activation of NMDA-receptors elicits "fictive locomotion" in lamprey spinal cord in vitro. Acta Physiol Scand 113:549–551. https://doi.org/10.1111/j.1748-1716.1981.tb06937.x

Harris-Warrick RM (2010) General principles of rhythmogenesis in central pattern generator networks. Prog Brain Res 187:213–222. https://doi.org/10.1016/b978-0-444-53613-6.00014-9

Hawthorne AL, Wylie CJ, Landmesser LT, Deneris ES, Silver J (2010) Serotonergic neurons migrate radially through the neuroepithelium by dynamin-mediated somal translocation. J Neurosci 30:420–430. https://doi.org/10.1523/jneurosci.2333-09.2010

Heckman CJ, Johnson M, Mottram C, Schuster J (2008) Persistent inward currents in spinal motoneurons and their influence on human motoneuron firing patterns. Neuroscientist 14:264–275. https://doi.org/10.1177/1073858408314986

Johnson MD (1994) Synaptic glutamate release by postnatal rat serotonergic neurons in microculture. Neuron 12:433–442. https://doi.org/10.1016/0896-6273(94)90283-6

Jordan LM (1998) Initiation of locomotion in mammals. Ann N Y Acad Sci 860:83–93. https://doi.org/10.1111/j.1749-6632.1998.tb09040.x

Jordan LM, Slawinska U (2011) Modulation of rhythmic movement: control of coordination. In: Gossard JP, Dubuc R, Kolta A (eds) Breathe, Walk and Chew: the neural challenge: Part Ii, pp 181–195

Jordan LM, Liu J, Hedlund PB, Akay T, Pearson KG (2008) Descending command systems for the initiation of locomotion in mammals. Brain Res Rev 57:183–191. https://doi.org/10.1016/j.brainresrev.2007.07.019

Josset N, Roussel M, Lemieux M, Lafrance-Zoubga D, Rastqar A, Bretzner F (2018a) Distinct contributions of mesencephalic locomotor region nuclei to locomotor control in the freely behaving mouse. Curr Biol. https://doi.org/10.1016/j.cub.2018.02.007

Josset N, Roussel M, Lemieux M, Lafrance-Zoubga D, Rastqar A, Bretzner F (2018b) Distinct contributions of mesencephalic locomotor region nuclei to locomotor control in the freely behaving mouse. Curr Biol 28:884–901. https://doi.org/10.1016/j.cub.2018.02.007

Kawashima T (2018) The role of the serotonergic system in motor control. Neurosci Res 129:32–39. https://doi.org/10.1016/j.neures.2017.07.005

Kiehn O, Quinlan KA, Restrepo CE, Lundfald L, Borgius L, Talpalar AE, Endo T (2008) Excitatory components of the mammalian locomotor CPG. Brain Res Rev 57:56–63. https://doi.org/10.1016/j.brainresrev.2007.07.002

Kjaerulff O, Kiehn O (2001) 5-HT modulation of multiple inward rectifiers in motoneurons in intact preparations of the neonatal rat spinal cord. J Neurophysiol 85:580–593. https://doi.org/10.1152/jn.2001.85.2.580

Kudo N, Yamada T (1987) N-methyl-D, L-aspartate-induced locomotor activity in a spinal cord-hindlimb muscles preparation of the newborn rat studied in vitro. Neurosci Lett 75:43–48. https://doi.org/10.1016/0304-3940(87)90072-3

MacLean JN, Schmidt BJ (2001) Voltage-sensitivity of motoneuron NMDA receptor channels is modulated by serotonin in the neonatal rat spinal cord. J Neurophysiol 86:1131–1138

MacLean JN, Cowley KC, Schmidt BJ (1998) NMDA receptor-mediated oscillatory activity in the neonatal rat spinal cord is serotonin dependent. J Neurophysiol 79:2804–2808. https://doi.org/10.1152/jn.1998.79.5.2804

Meijering E, Jacob M, Sarria JC, Steiner P, Hirling H, Unser M (2004) Design and validation of a tool for neurite tracing and analysis in fluorescence microscopy images. Cytometry A 58:167–176. https://doi.org/10.1002/cyto.a.20022

Mena-Segovia J, Bolam JP (2017) Rethinking the pedunculopontine nucleus: from cellular organization to function. Neuron 94:7–18. https://doi.org/10.1016/j.neuron.2017.02.027

Molliver ME (1987) Serotonergic neuronal systems: what their anatomic organization tells us about function. J Clin Psychopharmacol 7:3s–23s

Noga BR, Fortier PA, Kriellaars DJ, Dai X, Detillieux GR, Jordan LM (1995) Field potential mapping of neurons in the lumbar spinal cord activated following stimulation of the mesencephalic locomotor region. J Neurosci 15:2203–2217

Noga BR, Kriellaars DJ, Brownstone RM, Jordan LM (2003) Mechanism for activation of locomotor centers in the spinal cord by stimulation of the mesencephalic locomotor region. J Neurophysiol 90:1464–1478. https://doi.org/10.1152/jn.00034.2003

Noga BR, Johnson DMG, Riesgo MI, Pinzon A (2009) Locomotor-activated neurons of the cat. I. Serotonergic innervation and co-localization of 5-HT7, 5-HT2A, and 5-HT1A receptors in the thoraco-lumbar spinal cord. J Neurophysiol 102:1560–1576. https://doi.org/10.1152/jn.91179.2008

Noga BR, Sanchez FJ, Villamil LM et al (2017a) LFP oscillations in the mesencephalic locomotor region during voluntary locomotion. Front Neural Circuits 11:34. https://doi.org/10.3389/fncir.2017.00034

Noga BR, Turkson RP, Xie S, Taberner A, Pinzon A, Hentall ID (2017b) Monoamine release in the cat lumbar spinal cord during fictive locomotion evoked by the mesencephalic locomotor region. Front Neural Circuits 11:59. https://doi.org/10.3389/fncir.2017.00059

Ogawa Sachie K, Cohen Jeremiah Y, Hwang D, Uchida N, Watabe-Uchida M (2014) Organization of monosynaptic inputs to the serotonin and dopamine neuromodulatory systems. cell reports 8:1105–1118. https://doi.org/10.1016/j.celrep.2014.06.042

Perrier J-F, Cotel F (2015) Serotonergic modulation of spinal motor control. Curr Opin Neurobiol 33:1–7. https://doi.org/10.1016/j.conb.2014.12.008

Pose I, Sampogna S, Chase MH, Morales FR (2000) Cuneiform neurons activated during cholinergically induced active sleep in the cat. J Neurosci 20:3319–3327

Powers RK, Binder MD (2003) Persistent sodium and calcium currents in rat hypoglossal motoneurons. J Neurophysiol 89:615–624. https://doi.org/10.1152/jn.00241.2002

Robinson RB, Siegelbaum SA (2003) Hyperpolarization-activated cation currents: from molecules to physiological function. Annu Rev Physiol 65:453–480. https://doi.org/10.1146/annurev.physiol.65.092101.142734

Ros H, Magill PJ, Moss J, Bolam JP, Mena-Segovia J (2010) Distinct types of non-cholinergic pedunculopontine neurons are differentially modulated during global brain states. Neuroscience 170:78–91. https://doi.org/10.1016/j.neuroscience.2010.06.068

Roseberry TK, Lee AM, Lalive AL, Wilbrecht L, Bonci A, Kreitzer AC (2016) Cell-type-specific control of brainstem locomotor circuits by basal ganglia. Cell 164:526–537. https://doi.org/10.1016/j.cell.2015.12.037

Ryczko D, Auclair F, Cabelguen JM, Dubuc R (2016) The mesencephalic locomotor region sends a bilateral glutamatergic drive to hindbrain reticulospinal neurons in a tetrapod. J Comp Neurol 524:1361–1383. https://doi.org/10.1002/cne.23911

Schmidt BJ, Jordan LM (2000) The role of serotonin in reflex modulation and locomotor rhythm production in the mammalian spinal cord. Brain Res Bull 53:689–710. https://doi.org/10.1016/S0361-9230(00)00402-0

Scott MM, Wylie CJ, Lerch JK et al (2005) A genetic approach to access serotonin neurons for in vivo and in vitro studies. Proc Natl Acad Sci USA 102:16472–16477. https://doi.org/10.1073/pnas.0504510102

Shefchyk SJ, Jell RM, Jordan LM (1984) Reversible cooling of the brainstem reveals areas required for mesencephalic locomotor region evoked treadmill locomotion. Exp Brain Res 56:257–262. https://doi.org/10.1007/BF00236281

Shik ML, Severin FV, Orlovskii GN (1966) Control of walking and running by means of electric stimulation of the midbrain. Biofizika 11:659–666. https://doi.org/10.4097/kjae.2012.62.3.230

Slawinska U, Miazga K, Jordan LM (2014) The role of serotonin in the control of locomotor movements and strategies for restoring locomotion after spinal cord injury. Acta Neurobiol Exp (Wars) 74:172–187

Steeves JD, Jordan LM (1980) Localization of a descending pathway in the spinal cord which is necessary for controlled treadmill locomotion. Neurosci Lett 20:283–288. https://doi.org/10.1016/0304-3940(80)90161-5

Steeves JD, Jordan LM (1984) Autoradiographic demonstration of the projections from the mesencephalic locomotor region. Brain Res 307:263–276. https://doi.org/10.1016/0006-8993(84)90480-3

Takakusaki K, Habaguchi T, Ohtinata-Sugimoto J, Saitoh K, Sakamoto T (2003) Basal ganglia efferents to the brainstem centers controlling postural muscle tone and locomotion: a new concept for understanding motor disorders in basal ganglia dysfunction. Neuroscience 119:293–308. https://doi.org/10.1016/S0306-4522(03)00095-2

Takakusaki K, Chiba R, Nozu T, Okumura T (2016) Brainstem control of locomotion and muscle tone with special reference to the role of the mesopontine tegmentum and medullary reticulospinal systems. J Neural Transm (Vienna) 123:695–729. https://doi.org/10.1007/s00702-015-1475-4

Takeuchi Y, Kimura H, Sano Y (1982) Immunohistochemical demonstration of the distribution of serotonin neurons in the brainstem of the rat and cat. Cell Tissue Res 224:247–267. https://doi.org/10.1007/BF00216872

VanderHorst GJMV, Ulfhake B (2006) The organization of the brainstem and spinal cord of the mouse: relationships between monoaminergic, cholinergic, and spinal projection systems. J Chem Neuroanat 31:2–36. https://doi.org/10.1016/j.jchemneu.2005.08.003

Wang HL, Morales M (2009) Pedunculopontine and laterodorsal tegmental nuclei contain distinct populations of cholinergic, glutamatergic and GABAergic neurons in the rat. Eur J Neurosci 29:340–358. https://doi.org/10.1111/j.1460-9568.2008.06576.x

Whelan P, Bonnot A, O'Donovan MJ (2000) Properties of rhythmic activity generated by the isolated spinal cord of the neonatal

mouse. J Neurophysiol 84:2821–2833. https://doi.org/10.1152/jn.2000.84.6.2821

Wiklund L, Leger L, Persson M (1981) Monoamine cell distribution in the cat brain stem. A fluorescence histochemical study with quantification of indolaminergic and locus coeruleus cell groups. J Comp Neurol 203:613–647. https://doi.org/10.1002/cne.902030405

Yoo JH, Zell V, Wu J et al (2017) Activation of pedunculopontine glutamate neurons is reinforcing. J Neurosci 37:38–46. https://doi.org/10.1523/jneurosci.3082-16.2016

Zhou L, Liu M-Z, Li Q, Deng J, Mu D, Sun Y-G (2017) Organization of functional long-range circuits controlling the activity of serotonergic neurons in the dorsal raphe nucleus. Cell Rep 18(12):3018–3032. https://doi.org/10.1016/j.celrep.2017.02.077